Scientia Iranica B (2017) 24(2), 662–672

SCIENTIA IRANICA

Sharif University of Technology
Scientia Iranica
Transactions B: Mechanical Engineering
www.scientiairanica.com

Improving lateral dynamic of vehicle using direct yaw moment controller by differential brake torques based on quantitative feedback theory

M. Goharimanesh and A.A. Akbari*

Department of Mechanical Engineering, Ferdowsi University of Mashhad, Mashhad, Iran.

Received 10 August 2015; received in revised form 12 March 2016; accepted 4 July 2016

KEYWORDS
Robust control;
Quantitative feedback theory;
Direct yaw moment;
Vehicle stability control;
Differential brakes.

Abstract. In this paper, a robust controller based on quantitative feedback theory is designed to improve the lateral dynamic of a four-wheel vehicle using direct yaw moment controller. The essential yaw moment is calculated by this robust and applied to the vehicle dynamics model using a differential brake system, which is allocated by a rule-based controller. Quantitative feedback theory controller design is based on bicycle model which is assumed as a simple linear handling model. Herein, simulations are carried out based on nonlinear handling dynamics. To examine the controller in an almost real environment, CARSIM software is used to face a challenging maneuver. The results show that the robust controller could overcome the system uncertainties and control the vehicle in various handling maneuvers. Meanwhile, the braking torque allocated by differential brake systems is accessible and reliable for a real vehicle.

1. Introduction

One of the most important techniques to enhance the stability of the vehicle is the direct yaw moment control [1,2]. Direct Yaw Control (DYC) has been used in improving different vehicle control systems such as four-wheel steer vehicle [3], semi-trailer braking performance [4], active rear wheel steering for making a robust chassis system [5], four-wheel steering [6], considering the cross wind [7], and active differential to produce the required moment [8,9]. In order to develop DYC, many control theories have been examined in the literature such as sliding mode [10], optimal theory [11], fuzzy logic [12], the Lyapunov method [13], $H2 - H\infty$. [14], and fuzzy-PID controller [15]. Recently, an intelligent controller based on fuzzy reinforcement learning has been applied as a direct yaw controller on heave vehicle [16]. The reinforcement learning was used to design the rules for a fuzzy set.

Quantitative feedback theory is a robust controller, proper for the systems encountered by uncertainties. The first application of this theory was introduced for landing gear control [17]. Designing controller via this method is a trial and error task and is not straightforward [18]. There are a number of MATLAB toolboxes for designing the controller by this method [19-21]. Using some evolutionary algorithms, e.g. the genetic algorithm, could progress the loop shaping step [22]. In automotive technology, QFT has been employed to many systems [23] such as suspension of vehicle [24], suspension for heavy vehicles [25], semi-active suspension [26], and active steering control [27].

In vehicle dynamics, many parameters, like changing mass of vehicle or the position of center of gravity, increasing or decreasing the tire inflation pressure, can cause uncertainties. These uncertainties may change the behavior of vehicle dynamics and decrease the capability of controller to improve the stability. In

*. *Corresponding author.*
E-mail address: akbari@um.ac.ir (A.A. Akbari)

order to overcome this challenge, a robust control approach based on quantitative feedback theory is exploited. QFT provides a reliable controller for nonlinear systems based on the linear models of the system. Using a diverse range of parameters for designing the controller with linear model could satisfy the potential of the designed compensator for improving the vehicle stability.

In this paper, Quantitative Feedback Theory (QFT) is used to enhance the vehicle stability. First, regardless of the non-linear models, the system uncertainties can be identified by using only the linear model derived physically from linear vehicle dynamics. Then, a well-known algorithm based on QFT is designed to overcome the structural uncertainties in nonlinear models [28].

The article is organized as follows: In Sections 2 and 3, vehicle dynamics and tire dynamics models are introduced in linear and nonlinear regimes. Section 4 represents the principles of controller designing. Also, the quantitative feedback theory controller is introduced in this section. In Section 5, the simulation results of direct yaw moment control and brake torques allocation are presented and discussed.

2. Vehicle dynamics model

In this paper, two vehicle dynamic models have been employed for simulating. First, a bicycle model with two degrees of freedom, i.e. yaw and lateral motion is utilized to design the QFT controller, and then a more elaborate model with three degrees of freedom comprising of aforementioned motion and roll motion is considered. Figure 1 illustrates the overall layout of a four-wheel vehicle and its side layout for bicycle model which is used as a linear vehicle dynamic model.

The bicycle model is given in Eqs. (1)-(6). The

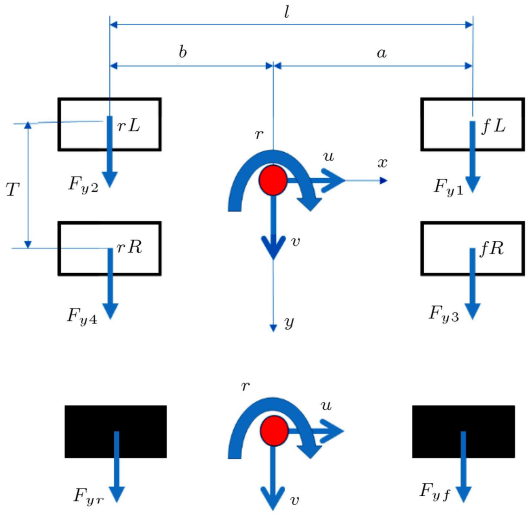

Figure 1. Vehicle geometrical properties.

derivation process of these formulas is discussed in the Appendix.

$$\begin{cases} \dot{X} = AX + BU \\ Y = CX + DU \end{cases} \tag{1}$$

$$X = \begin{bmatrix} v \\ r \end{bmatrix}, \quad U = \begin{bmatrix} \delta_f \\ M_c \end{bmatrix}, \tag{2}$$

$$A = -\begin{bmatrix} \frac{C_{\alpha f}+C_{\alpha r}}{mu} & \frac{aC_{\alpha f}-bC_{\alpha r}}{mu}+u \\ \frac{aC_{\alpha f}-bC_{\alpha r}}{I_z u} & \frac{a^2C_{\alpha f}+b^2C_{\alpha r}}{I_z u} \end{bmatrix}, \tag{3}$$

$$B = \begin{bmatrix} \frac{C_{\alpha f}}{m} & 0 \\ a\frac{C_{\alpha f}}{I_z} & \frac{1}{I_z} \end{bmatrix}, \tag{4}$$

$$C = \begin{bmatrix} 1 & 0 \\ 0 & 1 \end{bmatrix}, \tag{5}$$

$$D = \begin{bmatrix} 0 & 0 \\ 0 & 0 \end{bmatrix}. \tag{6}$$

In these linear set of ordinary differential equations, $X = [v\ r]^T$ is described as the lateral speed and the rotational speed, m is the total vehicle mass, I_z is the yaw moment of inertia, a and b are the distances from the center of gravity to the front and rear axles, respectively, and $C_{\alpha f}$, and $C_{\alpha r}$ are the lateral tire stiffness for the front and rear tires. In this basic model, u is the longitudinal speed which is considered to be a constant value. The corrective moment which is described as M_c is provided by controller law. This yaw moment can prevent the vehicle facing abnormal conditions. This state space has two inputs and two outputs. For this MIMO system, the transfer function between yaw rate and corrective moment can be shown in Eq. (7), where a_{ij} and b_{ij} are the arrays of matrices A and B introduced in state space form representation:

$$\frac{r(s)}{M_c(s)} = \frac{b_{22}s + (a_{21}b_{12} - a_{11}b_{22})}{s^2 - (a_{11}+a_{22})s + (a_{11}a_{22} - a_{12}a_{21})}. \tag{7}$$

For simulation purposes, it is necessary to add the roll motion as shown in Figure 2. By considering lateral, yaw and roll motions, a nonlinear model with three degrees of freedom is developed. The governing equations can be found in references [5].

The comprehensive model in this case is described as shown in Eqs. (8)-(10). Where F_y shows the lateral force for the each tire. Front and rear tires are addressed by f and r, respectively. Also, the right and left tires are presented by capital letters, R and L. In the following equations, m_s is the sprung mass and h' is the distance between the center of gravity and the roll center. Roll angle is defined by φ and the

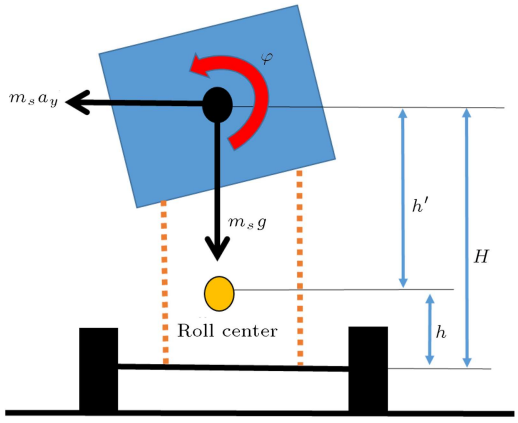

Figure 2. Roll motion of vehicle.

suspension stiffness and damping is presented by K_t and C_t, respectively:

$$\sum_{i=1}^{4} F_{yi} = ma_{yu} + m_s h'\ddot{\varphi}, \tag{8}$$

$$a\left(F_{y1}+F_{y3}\right) - b\left(F_{y2}+F_{y4}\right) + \frac{T}{2}\left(FX_1+F_{X2}\right) - \frac{T}{2}\left(FX_3+F_{x4}\right) = I_{zz}\dot{r}, \tag{9}$$

$$m_s g h' \sin(\varphi) - K_t\varphi - C_t\dot{\varphi} = I_{XXS}\ddot{\varphi} + m_s h' a_{yu}. \tag{10}$$

Meanwhile, the lateral acceleration introduced in Eq. (10) is described in Eq. (11):

$$a_y = \dot{v} + ur + \frac{m_s}{m}h'\ddot{\varphi}. \tag{11}$$

3. Tire dynamics model

In order to simulate the nonlinear regimes of the vehicle motion, the Magic Formula tire model with lateral slip is employed due to the capability of this model to simulate the limit handling situations where strong nonlinearities are present [29]. The lateral tire force can be expressed as in Eq. (12):

$$F_{yi} = f(\alpha_i F_{zi}), \tag{12}$$

where f is a non-linear function of the tire side slip angle and normal load F_{zi}. The lateral force is shown in Figure 3 for different values of normal forces. Normal forces described in Eq. (12) are shown in Eqs. (13-16):

$$F_{z1} = \frac{W}{2}\left(\frac{b}{L} - \frac{a_x}{g}\left(\frac{h}{L}\right) + K_R\left(\frac{a_y}{g}\left(\frac{h}{T}\right) - \left(\frac{m_s}{m}\right)\left(\frac{h'}{T}\right)\sin(\varphi)\right)\right), \tag{13}$$

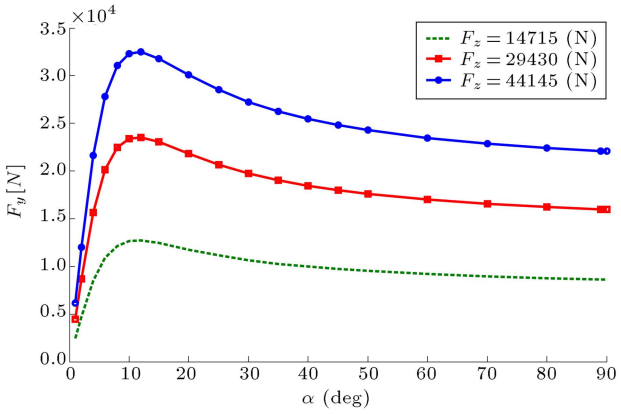

Figure 3. Lateral force versus sideslip angle in various values of normal force.

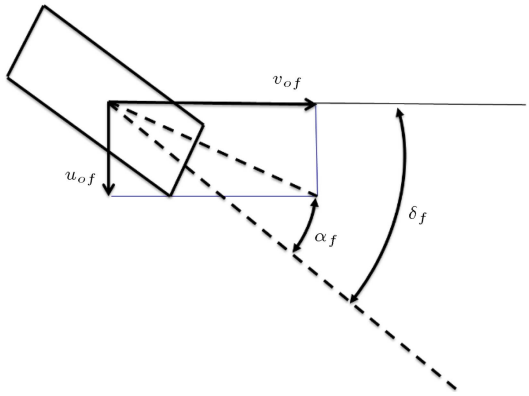

Figure 4. Sideslip angle for a tire.

$$F_{z2} = \frac{W}{2}\left(\frac{a}{L} + \frac{a_x}{g}\left(\frac{h}{L}\right) + (1-K_R)\left(\frac{a_y}{g}\left(\frac{h}{T}\right) - \left(\frac{m_s}{m}\right)\left(\frac{h'}{T}\right)\sin(\varphi)\right)\right), \tag{14}$$

$$F_{z3} = \frac{W}{2}\left(\frac{b}{L} - \frac{a_x}{g}\left(\frac{h}{L}\right) - K_R\left(\frac{a_y}{g}\left(\frac{h}{T}\right) - \left(\frac{m_s}{m}\right)\left(\frac{h'}{T}\right)\sin(\varphi)\right)\right), \tag{15}$$

$$F_{z4} = \frac{W}{2}\left(\frac{a}{L} + \frac{a_x}{g}\left(\frac{h}{L}\right) - (1-K_R)\left(\frac{a_y}{g}\left(\frac{h}{T}\right) - \left(\frac{m_s}{m}\right)\left(\frac{h'}{T}\right)\sin(\varphi)\right)\right). \tag{16}$$

Figure 4 illustrates Sideslip angle which is an important factor for tire forces. The sideslip angle formulas are given by Eqs. (17)-(20).

$$\alpha_1 = \delta_{T1} - tg^{-1}\left((v+ar)/(u+\frac{1}{2}Tr)\right), \tag{17}$$

$$\alpha_2 = \delta_{T2} - tg^{-1}\left((v-br)/(u+\frac{1}{2}Tr)\right), \tag{18}$$

$$\alpha_3 = \delta_{T3} - tg^{-1}\left((v+ar)/\left(u-\frac{1}{2}Tr\right)\right), \quad (19)$$

$$\alpha_4 = \delta_{T4} - tg^{-1}\left((v-br)/\left(u-\frac{1}{2}Tr\right)\right). \quad (20)$$

4. Controller design

The vehicle dynamics has uncertainties due to nonlinearity of its dynamics. Table 1 shows the vehicle parameter values and their uncertainties.

QFT employs a two-degree-of-freedom control structure which aims to shape the feedback and track responses independently. As shown in Figure 5, this control strategy uses unity feedback, a cascade compensator $G(s)$ which reduces the effects of uncertainties, a pre-filter $F(s)$ that shifts the response to the desired values and $P(s)$ which is an uncertain plant that belongs to a set $P(s) \in \{P(s,\alpha); \alpha \in \Phi\}$, where here α is the vector of uncertain parameters, which takes the values in φ.

In parametric uncertain systems, the principles of QFT controller design can be summarized as in the following steps [30]:

- Generating plant templates prior to the QFT design;
- QFT converts closed-loop magnitude specifications into magnitude constraints on a nominal open-loop function by using generated plant templates;
- A nominal open-loop function is then designed to simultaneously satisfy its constraints as well as to achieve nominal closed-loop stability.

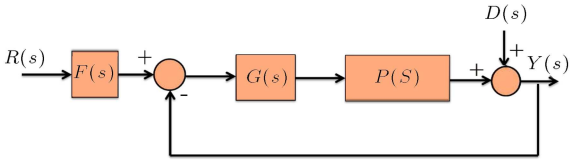

Figure 5. A typical unity feedback system.

QFT design includes three main steps which are computing the robust performance bounds, designing the robust control, and the proper pre-filter if there is a necessity for it. At the end, an analysis of the design is required. The main steps involved in the design of the controller are template generation, loop shaping, and manipulation of tolerance bounds within the available freedom, template size considerations, and selection of nominal transfer function matrices. In this paper, we employ the pre-mentioned steps for designing an optimal robust controller. The procedure of QFT controller is shown in Figure 6. To generate a template for QFT designing procedure, the proposed transfer function shown in Eq. (7) is used with all of the uncertainties which are introduced in Table 1. Figure 7 demonstrates the plant uncertainty in Nichols chart.

The magnitude of a closed-loop system is called robust margin and for all the uncertainties, its value as shown in Eq. (21) must be less than 1.1:

$$\left|\frac{P_1(j\omega)G(j\omega)}{1+P_1(j\omega)G(j\omega)}\right| \leq 1.1. \quad (21)$$

For all plant uncertainties, overshoot and settling time for robust tracking specification based on proper performance of the actuator is (=5%) and (=0.05s), respectively. Suitable disturbance rejection bounds to reduce the cross-coupling effects between the joints are shown in Eqs. (22)-(24). The robust tracking bounds

Figure 6. Quantitative feedback theory controller designing procedure.

Table 1. Vehicle parameters uncertainties.

Parameter description	Symbol	Uncertainties	Value
Sprung mass (kg)	m_s	1000-1600	1300
Unsprung mass (kg)	m_{us}	—	1100
Moment of inertia (kg m^2)	I_x	—	750
Moment of inertia (kg m^2)	I_z	2000-2600	2000
Track (m)	T		1.4
Distance from center of mass to front axle (m)	a	1.1-1.6	1.1
Distance from center of mass to rear axle (m)	b	0.9-1.4	1.4
Height of center of mass (m)	H	0.4-0.5	0.5
Distance from center of mass to roll center (m)	h'	—	0.4
Torsional stiffness (N.m/rad)	K_t	—	45000
Damping factor (N.m.s/rad)	C_t	—	2600
Road friction	μ	0.2-0.9	0.9

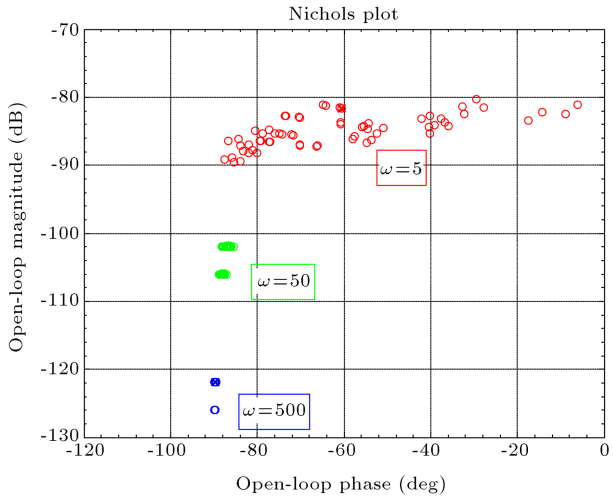

Figure 7. Uncertainty templates in Nichols chart.

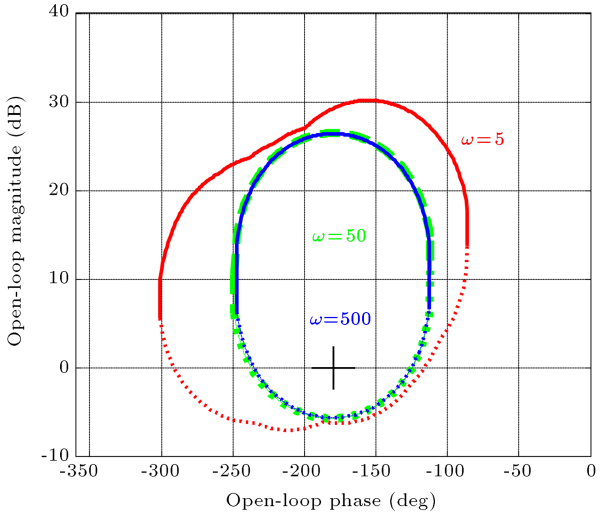

Figure 8. Disturbance rejections in Nichols chart.

are demonstrated in Figure 8:

$$T_{RL}(\omega) \leq \left| \frac{P_1(j\omega)G(j\omega)}{1+P(j\omega)G(j\omega)} \right| \leq T_{RU}(\omega), \tag{22}$$

$$T_{RL}(\omega) = \left| \frac{k\left(\frac{j\omega}{a}+1\right)}{\left(\frac{j\omega}{\omega_{n1}}\right)^2 + \frac{2\zeta}{\omega_{n1}}(j\omega)+1} \right|, \tag{23}$$

$$T_{RU}(\omega) = \left| \frac{1}{\left(\frac{j\omega}{\sigma_1}+1\right)} \right|. \tag{24}$$

Using MATLAB® QFT-Toolbox, which has been developed by Garcia-Sanz in 2012 [21], the controller is designed and applied to the system. Results demonstrate that the open-loop transfer function lies exactly on its robust performance bounds. The overall bounds of the design can be calculated by combining appropriately the individual bounds for each point of

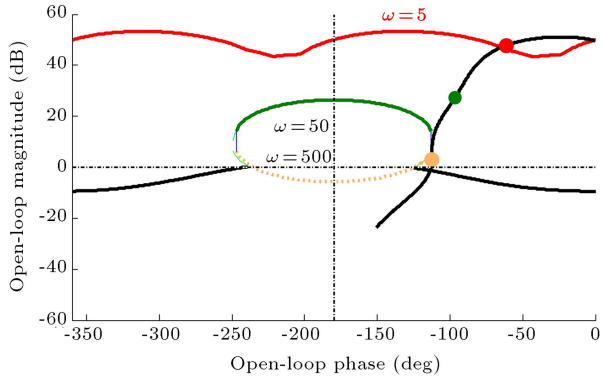

Figure 9. Loop-shaping in Nichols chart.

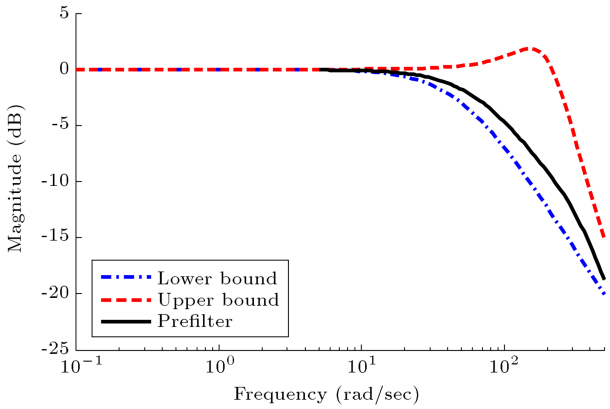

Figure 10. Pre-filter shaping with two lower and upper bounds for designing a robust controller.

the phase-grid and does not penetrate the U-contour at all frequency values ($j\omega$). The design of pre-filter guarantees the satisfaction of tracking specification. In Figures 9 and 10, loop shaping and pre-filter shaping of open-loop transfer function are shown, respectively. Therefore, we designed the optimal controller ($G(s)$) and pre-filter ($F(s)$) as shown in Eq. (25):

$$G(s) = k_1\left(\frac{s}{z_1}+1\right)\left(\frac{1}{\frac{s}{p_1}+1}\right)\left(\frac{1}{\frac{s}{p_2}+1}\right),$$

$$F(s) = k_2\left(\frac{1}{\frac{s}{p_3}+1}\right), \tag{25}$$

where $k_1 = 3e6$, $z_1 = 300$, $p_1 = 3000$, $p_2 = 160$, and $p_3 = 70$. We demonstrate the functionality of our controller (Figure 11) by investigating the step response of the controller.

5. Simulation and result

5.1. Direct yaw control

For vehicle handling simulation, a nonlinear model discussed in Section 2 is employed and modeled in SIMULINK environment. As Figure 12 shows, this model is equipped with steering angle and controller.

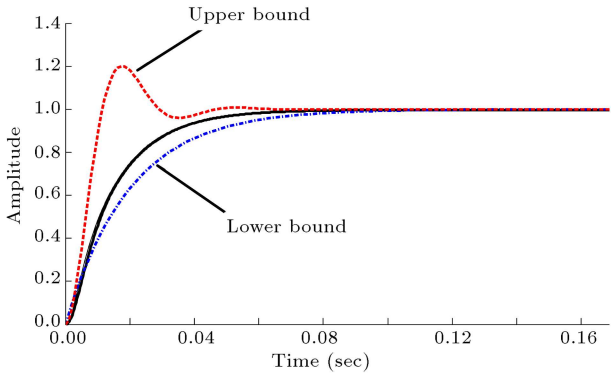

Figure 11. Step response of controller.

To simulate the nonlinear differential equations, Differential Algebraic Splitter (DAS), recently introduced as an organizing simulation method, was used [31]. DAS method can simplify the nonlinear differential equations easily. In this method, all of differential parts of equations are substituted by From-Goto blocks, and then will be integrated using the common Simulink integrator. The rest of the nonlinear equations are modeled algebraically without any integrator. Every equation is ended to a block where it is referred to the differential part of equation.

Desired yaw rate is used as a comparing value with output vehicle yaw rate. This value is introduced as a result of the function shown in Eq. (26):

$$r_d = \frac{u\delta}{l + K_{us}u^2}. \tag{26}$$

In this equation, r_d is desired yaw rate, u is longitudinal speed, δ is steering angle, l is wheelbase of vehicle, and K_{us} is the understeer gradient proposed 0.01 for this simulation. For a comprehensive simulation, three famous maneuvers, namely step, Lane change, and Fish hook steering are employed, as shown in Figure 13. These maneuvers are able to show the capability of vehicle controller for improving the stability. In this paper, it is proposed to have 120-degree turn of the steering wheel. Moreover, gear ratio is considered to be 20 in this simulation. So, the maximum value in steer as shown in Figure 13 is 6 degrees. The result of simulation for step steering is shown in Figure 14. In this simulation, the longitudinal speed for vehicle was assumed 100 km/h. This maneuver is examined and yaw rate is obtained with and without designed controller. $X - Y$ position is surveyed to show the effect of controller on vehicle path. Consequently, the controller is able to enhance the stability and track the desired yaw rate.

Quantitative feedback theory as described in the previous section meets the uncertainties and designs the controller and pre-filter to overcome all of the conditions. To show the robustness of the designed controller, the simulation conditions have been changed. The longitudinal speed becomes 140 km/h, the mass of vehicle increases to 1800 kg, and the center of gravity changes about 30 cm to the rear of vehicle. This changing condition was assumed to show the instability condition for a vehicle. Moreover, to clarify the controller's influence, two other maneuvers which are more aggressive than step steering are investigated. The results of these simulations are shown in Figure 15. The yaw rate graph confirms the effectiveness of the controller. In both of these two maneuvers, vehicle without controller cannot track the desired yaw rate which was assumed for that simulation, whereas the QFT controller can overcome the uncertainties and meet the desired path.

5.2. *Differential brakes*

In this section, the upper controller designed in the previous section delivers the yaw moment to the lower controller which may be a differential brake system. This technology is named ESP (Electronic Stability Program) in many vehicle manufacturers. To do the simulation in an approximately real environment, CARSIM software, which is well known in vehicle dynamics simulating, was employed. The maneuver

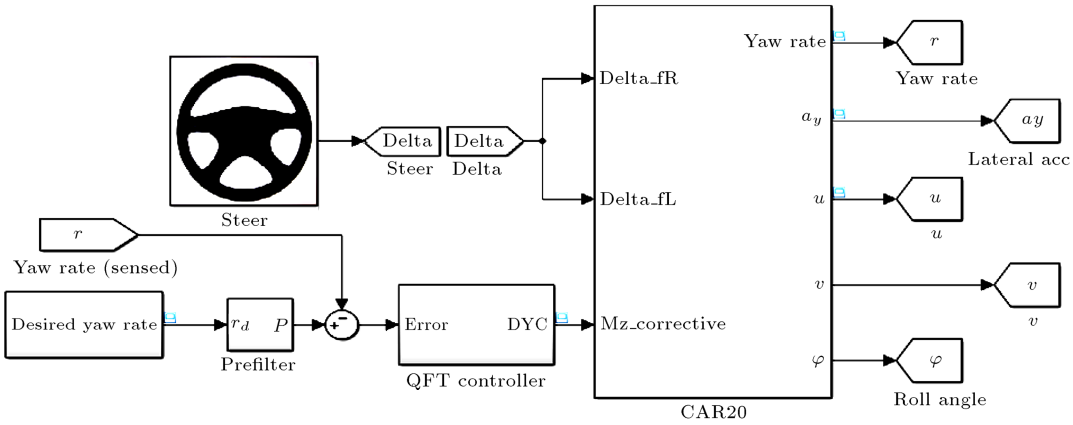

Figure 12. Nonlinear vehicle model in SIMULINK.

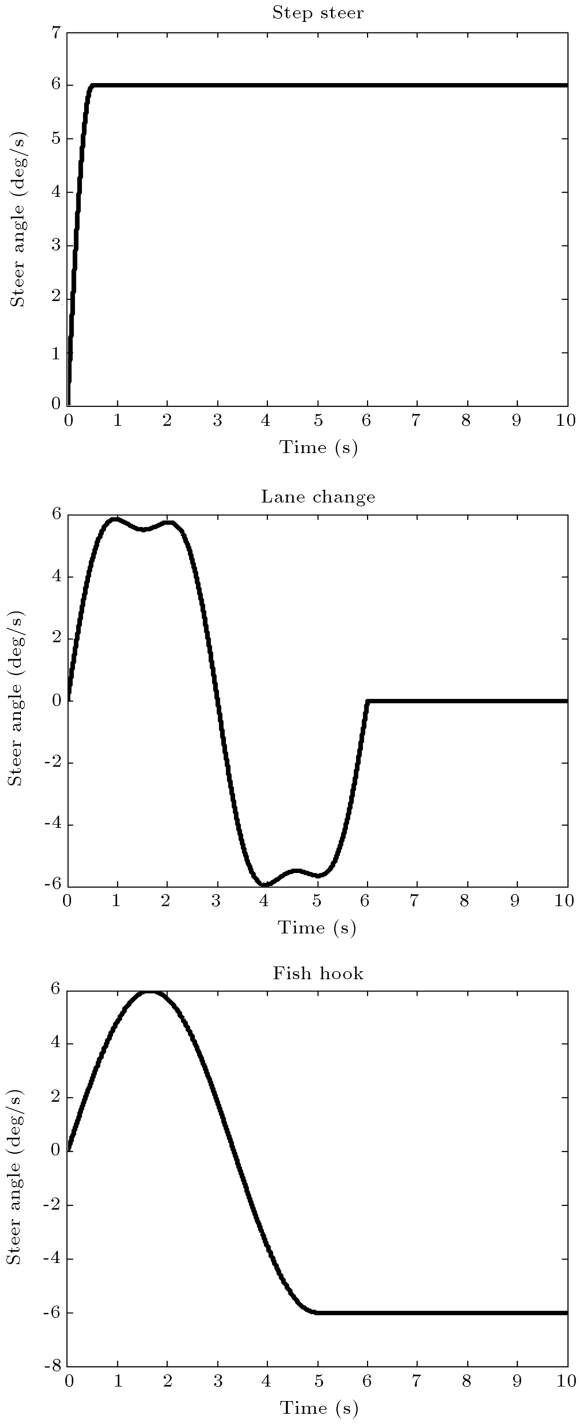

Figure 13. Three maneuver steering angles on front wheels.

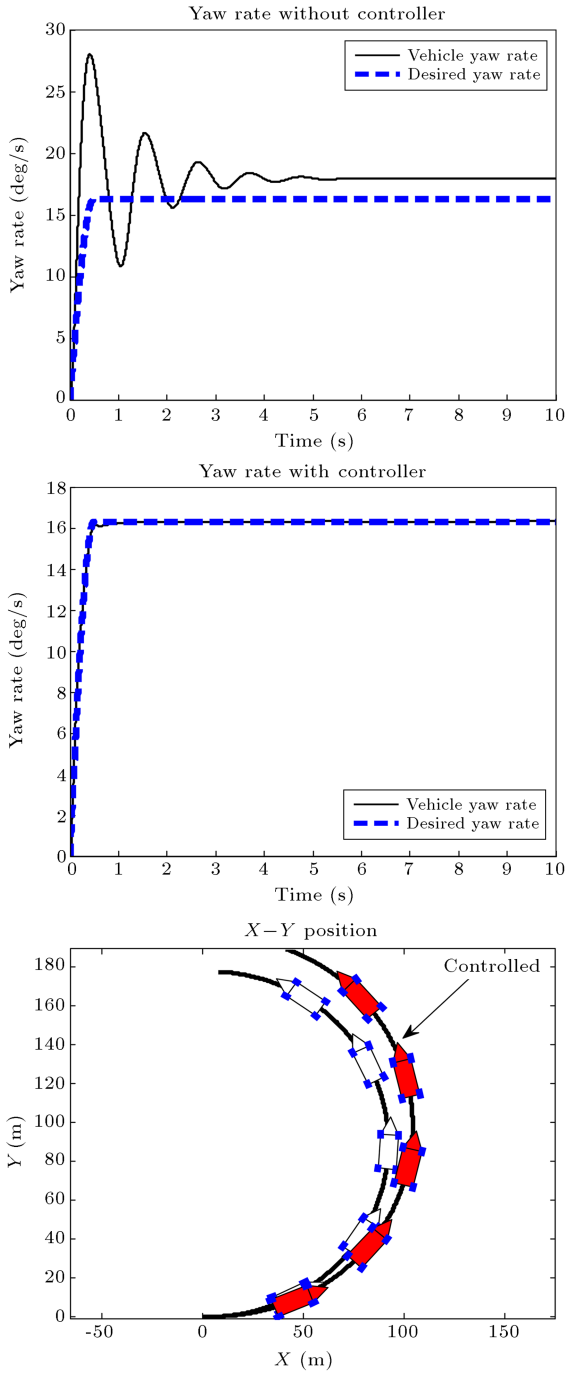

Figure 14. Result of simulation for step steering.

used in this simulation was "double lane change" which is an important maneuver for testing vehicle handling performance. The wheel steer for this maneuver is shown in Figure 16. The gear ratio for transforming this steer on the front wheel was considered 1/20.

The longitudinal speed was assumed as 80 km/hr, and the road friction was considered low around 0.5 which means a rainy road. The other conditions were the same as the last simulation considered in Section 5-1. The lower policy for brake torques allocation is so easy. When the yaw moment was achieved as negative, two right-hand tires started to brake; otherwise, two left-hand tires braked. The torque moment is calculated for each tire as $|M_c|R/T$, where M_c is the direct yaw moment calculated by the upper controller which is QFT in this study; R is the tire radius; and T is the track width of vehicle for the vehicle axis which are assumed 0.33 and 1.55 m, respectively.

In Figure 17, the direct yaw moment calculated by QFT is shown. As this figure illustrates, the value

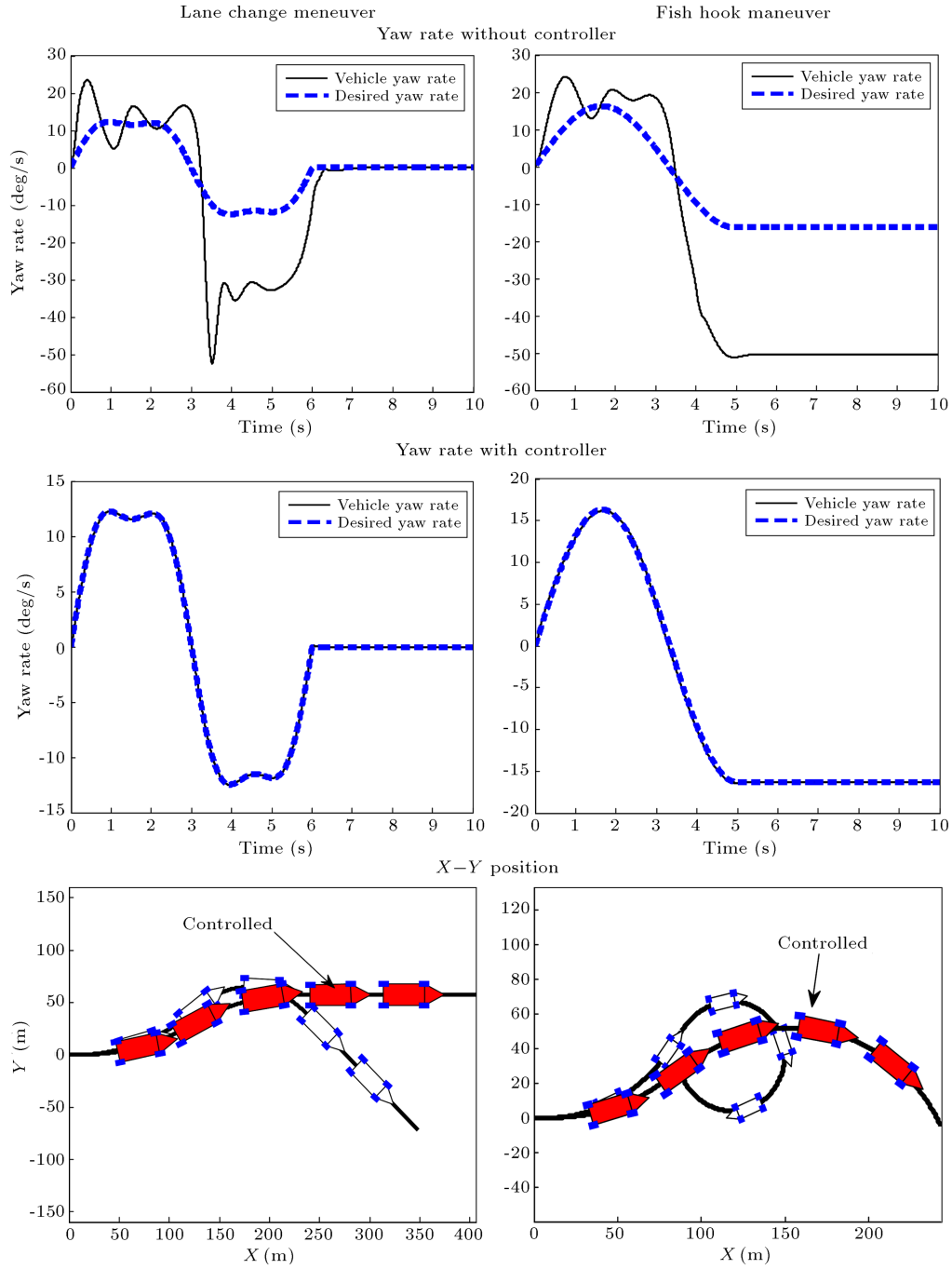

Figure 15. Result of simulation for robustness analysis.

for this moment is bounded in [-4000, 4000] Nm range. This interval is a reasonable torque which can be produced by some brakes in a four-wheel vehicle.

The brake tires calculated by the lower controller are shown in Figure 18. As discussed previously, when two right-hand tires start to brake, the others do not brake, and vice versa. This was achieved by a rule-based controller in Simulink environment where upper and lower controllers exist.

Using this brake torques allocation, the yaw rate controlled is compared with the uncontrolled vehicle and desired graph in Figure 19. Figure 20 shows the error of a controlled and uncontrolled vehicles for tracking desired yaw rate. The reliability of designed controller can be concluded from these error values.

6. Conclusion

In this paper, we enhanced the vehicle stability using external yaw moment control and then allocated tire braking torques. In order to apply the proposed method, firstly, a QFT controller must be designed

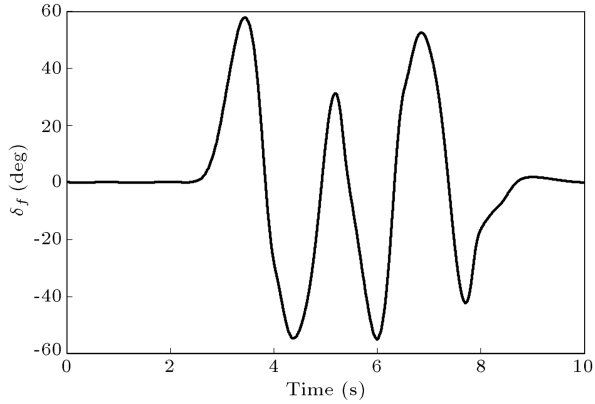

Figure 16. Wheel steer versus time in double lane change maneuver.

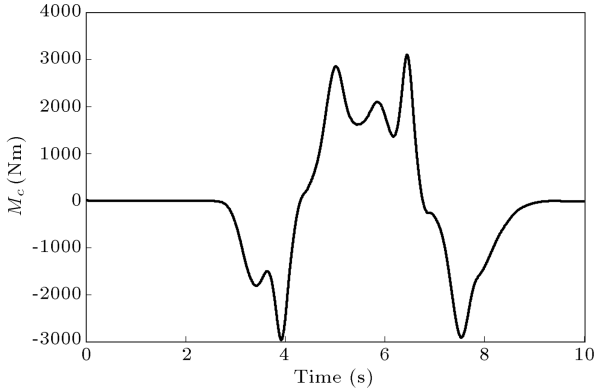

Figure 17. Direct yaw moment calculated by QFT in the simulation time.

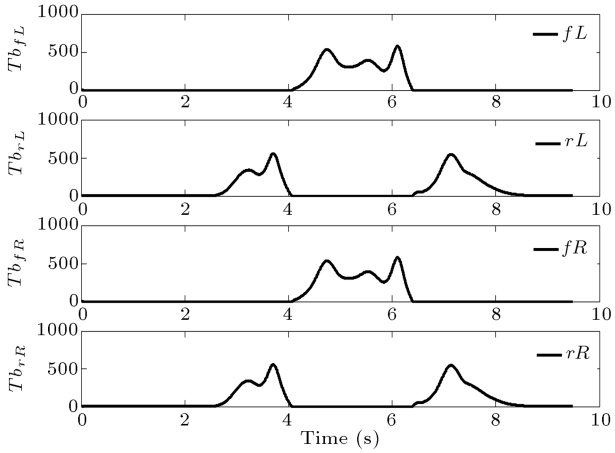

Figure 18. Brake torques calculated for each tire after calculating direct yaw moment.

based on the linear vehicle handling model of the system, and then a nonlinear model is employed to examine the achieved controller. To test the robustness of controller, some vehicle conditions were changed and some aggressive maneuvers were investigated. Moreover, the brake torques were allocated based on the direct yaw moment calculated by QFT controller. The results of this survey show that the proposed

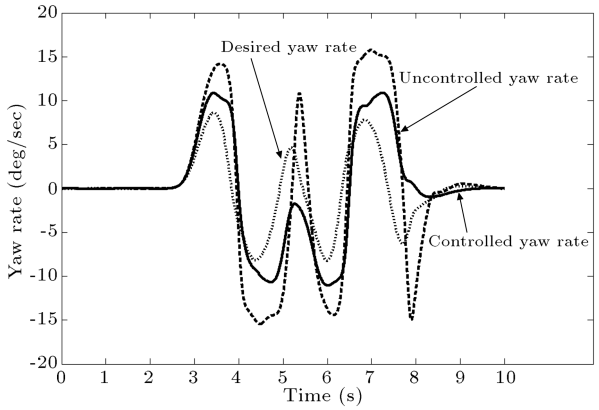

Figure 19. A comparison of yaw rate values for two controlled and uncontrolled vehicles.

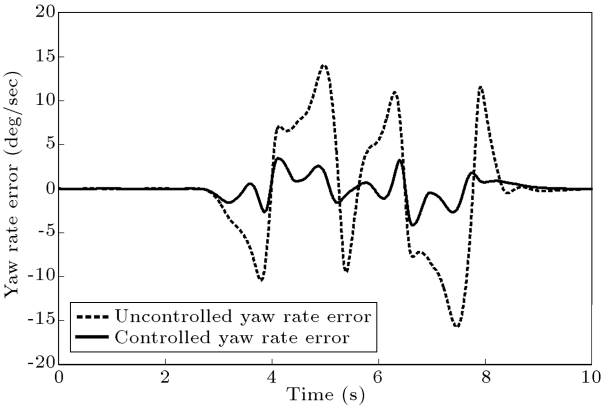

Figure 20. The yaw rate error produced by controlled and uncontrolled vehicles.

controller design using QFT with differential brakes has an excellent capability in controlling the vehicle dynamic system.

References

1. Shibahata, Y., Shimada, K. and Tomari, T. "Improvement of vehicle maneuverability by direct yaw moment control", *Veh. Syst. Dyn.*, **22**(5-6), pp. 465-481 (1993).
2. Van Zanten, A., Erhardt, R. and Pfaff, G. "VDC-the vehicle dynamics control system of Bosch", *ATZ*, **96**(11), p. 8 (1994).
3. Abe, M., Ohkubo, N. and Kano, Y. "A direct yaw moment control for improving limit performance of vehicle handling-comparison and cooperation with 4WS", *Veh. Syst. Dyn.*, **25**(S1), pp. 3-23 (1996).
4. Kano, Y., Sawai, M., Sato, T., Nanba, H., and Abe, M. *Improvement of Semi-trailer Braking Performance with Direct Yaw Moment Control*, JSAE Review, **18**(2), pp. 189-189 (1997).
5. Nagai, M., Hirano, Y. and Yamanaka, S. "Integrated control of active rear wheel steering and direct yaw moment control", *Veh. Syst. Dyn.*, **27**(5-6), pp. 357-370 (1997).

6. Abe, M. "Vehicle dynamics and control for improving handling and active safety: from four-wheel steering to direct yaw moment control", *Proc. Inst. Mech. Eng. K J. Multi-body Dyn.*, **213**(2), pp. 87-101 (1999).
7. Boada, B., Boada, M. and Diaz, V. "Yaw moment control for vehicle stability in a crosswind", *Int. J. Veh. Des.*, **39**(4), pp. 331-348 (2005).
8. Canale, M., Fagiano, L., Milanese, M. and Borodani, P. "Robust vehicle yaw control using an active differential and IMC techniques", *Control Eng. Pract.*, **15**(8), pp. 923-941 (2007).
9. Mashadi, B., Mostaani, S. and Majidi, M. "Vehicle stability enhancement by using an active differential", *Proc. Inst. Mech. Eng. I J. Syst. Control Eng.*, **225**, pp. 1-17 (2011).
10. Yoshioka, T., Adachi, T., Butsuen, T., Okazaki, H. and Mochizuki, H. "Application of sliding-mode theory to direct yaw-moment control", *JSAE Review*, **20**(4), pp. 523-529 (1999).
11. Esmailzadeh, E., Goodarzi, A. and Vossoughi, G.R. "Optimal yaw moment control law for improved vehicle handling", *Mechatronics*, **13**(7), pp. 659-675 (2003).
12. Tahami, F., Farhangi, S. and Kazemi, R. "A fuzzy logic direct yaw-moment control system for all-wheel-drive electric vehicles", *Veh. Syst. Dyn.*, **41**(3), pp. 203-221 (2004).
13. Ding, N. and Taheri, S. "An adaptive integrated algorithm for active front steering and direct yaw moment control based on direct Lyapunov method", *Veh. Syst. Dyn.*, **48**(10), pp. 1193-1213 (2010).
14. HU, A.-J. and WANG, Z.-H. "H_2/H_∞ control for integrated active front steering and direct yaw moment", *J. Henan Univ. Sci. Tech. (Nat Sci)*, **6**, p. 008 (2010).
15. Liu, C., Meng, Y., Zhang, B. and Fu, Y. "Fuzzy-PID control of four-wheel steering with direct yaw-moment", *Machinery & Electronics*, **11**, p. 014 (2010).
16. Akbari, A.A. and Goharimanesh, M. "Yaw moment control using fuzzy reinforcemnt learning", *AVEC14*, Japan: JSAE (2014).
17. Clough, B.T., Horowitz, I. and Houpis, C. "Robust control design for short take-off landing gear (STOL) aircraft using quantitative feedback theory", *NAECON*, USA: IEEE (1986).
18. Li, A., et al. "Applying quantitative feedback theory (QFT) to designing controller for flexible flight vehicle", *J. NPU*, **28**(6), pp. 916-920 (2010).
19. Borghesani, C., Chait, Y. and Yaniv, O. "Quantitative feedback theory toolbox for use with MATLAB®: User's guide", *MathWorks, Incorporated* (1994).
20. Nataraj, P.S.V. "A MATLAB toolbox for QFT-based synthesis of linear.nonlinear lumped and linear distributed systems", *CACSD*, USA: IEEE (1994).
21. Garcia-Sanz, M. and Houpis, C.H., *Wind Energy Systems: Control Engineering Design*, CRC Press (2012).
22. Wenhua Chen, D.J.B. "Automatic loop-shaping in qft using genetic algorithms", in *Proc. of 3rd Asia-Pacific Conf. on Cont. & Meas.* (1998).
23. Slicker, J.M. and Loh, R.N.K. "Design of robust vehicle launch control system", *IEEE Ttansactions on Control Systems Technology*, **4**(4), pp. 326-335 (1996).
24. Liberzon, A., Rubinstein, D. and Gutman, P.O. "Active suspension for single wheel station of off-road track vehicle", *Int. J. Robust Nonlin. Control*, **11**(10), pp. 977-999 (2001).
25. Rajapakse, N.I., Happawana, G.S. and Hurmuzlu, Y. "Suppression of heavy-truck driver-seat vibration using sliding-mode control and quantitative feedback theory", *Proc. Inst. Mech. Eng. I J. Syst. Control Eng.*, **221**(5), pp. 769-779 (2007).
26. Zapateiro, M., Pozo, F., Karimi, H. and Luo, N. "Semi-active control methodologies for suspension control with magnetorheological dampers", *IEEE/ASME T. Mech.*, **17**(2), pp. 370-380 (2011).
27. Zhang, J., Kim, J., Xuan, D. and Kim, Y. "Design of active front steering (AFS) system with QFT control", *Int. J. Comput. Appl. T.*, **41**(3-4), pp. 236-245 (2011).
28. Horowitz, I. "Quantitative feedback theory", *IEE Proc. D*, **129**(6), pp. 215-226 (1982).
29. Pacejka, H., *Tyre and Vehicle Dynamics*, **642**, Elsevier (2005).
30. Horowitz, I. "Survey of quantitative feedback theory (QFT)", *Int. J. Robust Nonlin. Control*, **11**(10), pp. 887-921 (2001).
31. Goharimanesh, M. and Akbari, A. "Optimum parameters of nonlinear integrator using design of experiments based on Taguchi method", *J. Comput. Appl. Mech.*, **46**(2), pp. 233-241 (2015).

Appendix

In this part a linear vehicle dynamic model named bicycle is derived as follows:

$$\sum F_y = ma_y,$$

$$\sum M_z = I_z\dot{r},$$

$$F_{yf} + F_{yr} = m(\dot{v} + ur),$$

$$aF_{yf} - bF_{yr} + M_c = I_z\dot{r},$$

$$F_{yf} = C_{\alpha f}\alpha_f,$$

$$F_{yr} = C_{\alpha r}\alpha_r,$$

$$\alpha_f = \delta_f - \tan^{-1}\left(\frac{v_{of}}{u_{of}}\right) = \delta_f - \frac{v_{of}}{u_{of}}$$

$$= \delta_f - \frac{v + ar}{u},$$

$$\alpha_r = \delta_r - \tan^{-1}\left(\frac{v_{or}}{u_{or}}\right) = 0 - \tan^{-1}\left(\frac{v_{or}}{u_{or}}\right) = 0$$

$$-\frac{v_{or}}{u_{or}} = -\frac{v - br}{u},$$

$$\begin{bmatrix} m & 0 \\ 0 & I_z \end{bmatrix} \begin{bmatrix} \dot{v} \\ \dot{r} \end{bmatrix} + \begin{bmatrix} \frac{C_{af}+C_{ar}}{u} & \frac{aC_{af}-bC_{ar}}{u} + mu \\ \frac{aC_{af}-bC_{ar}}{u} & \frac{a^2C_{af}+b^2C_{ar}}{u} \end{bmatrix} \begin{bmatrix} v \\ r \end{bmatrix}$$

$$= \begin{bmatrix} C_{af} \\ aC_{af} \end{bmatrix} \delta_f + \begin{bmatrix} 0 \\ 1 \end{bmatrix} M_c \begin{bmatrix} \dot{v} \\ \dot{r} \end{bmatrix} =$$

$$- \begin{bmatrix} \frac{C_{af}+C_{ar}}{mu} & \frac{aC_{af}-bC_{ar}}{mu} + u \\ \frac{aC_{af}-bC_{ar}}{I_z u} & \frac{a^2C_{af}+b^2C_{ar}}{I_z u} \end{bmatrix} \begin{bmatrix} v \\ r \end{bmatrix}$$

$$+ \begin{bmatrix} \frac{C_{af}}{m} & 0 \\ a\frac{C_{af}}{I_z} & \frac{1}{I_z} \end{bmatrix} \begin{bmatrix} \delta_f \\ M_c \end{bmatrix}.$$

Biographies

Masoud Goharimanesh received his BS and MS degrees in Mechanical Engineering and Automotive Engineering from Islamic Azad University of Mashhad and Iran University of Science and Technology, respectively. He is currently a PhD Student in Ferdowsi University of Mashhad. His research fields include vehicle dynamics, control engineering, reinforcement learning, and soft computing, especially on complex nonlinear systems.

Ali Akbar Akbari received a PhD degree in Manufacturing Engineering from Chiba University, Japan, in 2003. He is currently an Associated Professor with the Mechanical Department, Ferdowsi University of Mashhad, Iran. His research interests include robotics, manufacturing engineering, and control engineering.